

Coherent excitations and electron-phonon coupling in Ba/EuFe₂As₂ compounds investigated by fem to second time- and angle-resolved photoemission spectroscopy

I. Avigo, R. Cortés, L. Rettig, S. Thirupathaiah, H. S. Jeevan, Philipp Gegenwart, T. Wolf, M. Ligges, M. Wolf, J. Fink, U. Bovensiepen

Angaben zur Veröffentlichung / Publication details:

Avigo, I., R. Cortés, L. Rettig, S. Thirupathaiah, H. S. Jeevan, Philipp Gegenwart, T. Wolf, et al. 2013. "Coherent excitations and electron-phonon coupling in Ba/EuFe₂As₂ compounds investigated by fem to second time- and angle-resolved photoemission spectroscopy." *Journal of Physics: Condensed Matter* 25 (9): 094003. <https://doi.org/10.1088/0953-8984/25/9/094003>.

Coherent excitations and electron–phonon coupling in Ba/EuFe₂As₂ compounds investigated by femtosecond time- and angle-resolved photoemission spectroscopy

I Avigo¹, R Cortés^{2,3,7}, L Rettig^{1,2}, S Thirupathaiah⁴, H S Jeevan⁵, P Gegendwart⁵, T Wolf⁶, M Ligges¹, M Wolf³, J Fink⁴ and U Bovensiepen^{1,8}

¹ Fakultät für Physik, Universität Duisburg–Essen, Lotharstr. 1, D-47048 Duisburg, Germany

² Fachbereich Physik, Freie Universität Berlin, Arnimallee 14, D-14195 Berlin, Germany

³ Abteilung Physikalische Chemie, Fritz-Haber-Institut d. MPG, Faradayweg 4-6, D-14195 Berlin, Germany

⁴ Leibniz-Institute for Solid State and Materials Research Dresden, P O Box 270116, D-01171 Dresden, Germany

⁵ I Physikalisches Institut, Georg-August Universität Göttingen, D-37077 Göttingen, Germany

⁶ Karlsruhe Institute of Technology, Institut für Festkörperphysik, D-76021 Karlsruhe, Germany

E-mail: uwe.bovensiepen@uni-due.de

Abstract

We employed femtosecond time- and angle-resolved photoelectron spectroscopy to analyze the response of the electronic structure of the 122 Fe-pnictide parent compounds Ba/EuFe₂As₂ and optimally doped BaFe_{1.85}Co_{0.15}As₂ near the Γ point to optical excitation by an infrared femtosecond laser pulse. We identify pronounced changes of the electron population within several 100 meV above and below the Fermi level, which we explain as a combination of (i) coherent lattice vibrations, (ii) a hot electron and hole distribution, and (iii) transient modifications of the chemical potential. The responses of the three different materials are very similar. In the coherent response we identify three modes at 5.6, 3.3, and 2.6 THz. While the highest frequency mode is safely assigned to the A_{1g} mode, the other two modes require a discussion in comparison to the literature. Employing a transient three temperature model we deduce from the transient evolution of the electron distribution a rather weak, momentum-averaged electron–phonon coupling quantified by values for $\lambda(\omega^2)$ between 30 and 70 meV². The chemical potential is found to present pronounced transient changes reaching a maximum of 15 meV about 0.6 ps after optical excitation and is modulated by the coherent phonons. This change in the chemical potential is particularly strong in a multiband system like the 122 Fe-pnictide compounds investigated here due to the pronounced variation of the electron density of states close to the equilibrium chemical potential.

1. Introduction

The discovery of high- T_c superconductivity in F doped LaFeAsO [1] led to an almost immediate discovery of further

FeAs-based superconductors with transition temperatures T_c up to 55 K. While the superconducting pairing mechanism in conventional superconductors is related to electron–phonon coupling, the current thinking is that the iron pnictides (FePn), similarly to the cuprate superconductors, belong to the class of unconventional superconductors, in which the mechanism is possibly related to correlation effects and/or magnetic

⁷ Present address: Centre for Functional Nanomaterials, Brookhaven National Laboratory, Upton, NY 11973, USA.

⁸ www.uni-due.de/agbovensiepen.

excitations [2]. Although there are various similarities between cuprates and FePns, e.g. the nearness in the phase diagram of antiferromagnetism and superconductivity, there are also differences. While in the cuprates the parent compounds are antiferromagnetic Mott–Hubbard insulators, in the FePns the parent compounds are antiferromagnetic metals which indicates that the correlation effects in the latter systems are reduced. This view is supported by, e.g., x-ray absorption and photoemission spectroscopy on FePns resulting in a weakly correlated electronic structure with a moderate value of the on-site Coulomb interaction $U \approx 1.5$ eV [3–6].

On the other hand, there is no real consensus on the mechanism of high- T_c superconductivity in FePns and on the role of electron–phonon coupling. Experiments on the isotope effect in these compounds exhibit conflicting results [2]. Theoretical calculations on the electron–phonon coupling constant λ yielded for the non-magnetic and antiferromagnetic systems $\lambda \approx 0.2$ and $\lambda < 0.35$, respectively [7, 8]. Optical pump–probe studies with femtosecond time resolution analyzed λ by determining the second moment of the Eliashberg electron–phonon coupling function $\lambda\langle\omega^2\rangle$ through the rate of energy transfer from the optically excited electrons to phonons [9, 10]. Although the reported results vary in detail due to different assumptions regarding ω , the resulting electron–phonon coupling constant λ is found to be 0.1–0.2. In our recent femtosecond time- and angle-resolved photoemission spectroscopy (trARPES) study [11], in which ultrashort light pulses in the UV spectral range were used, we derived for the second moment of the Eliashberg electron–phonon coupling function $\lambda\langle\omega^2\rangle = 90 \pm 40$ meV². Using an average phonon frequency $\langle\omega\rangle \approx 20$ meV/ \hbar a value of $\lambda < 0.2$ can be derived from this result. Although these electron–phonon coupling constants are small, which makes it difficult to explain T_c values above 20 K by electron–phonon coupling, there is no consensus on the role of phonons in the mechanism of superconductivity in FePns. Therefore information on phonons and their coupling to the charge carriers is vitally important. Accordingly we present here further results on the coherent excitations of phonons and on the electron–phonon coupling in undoped Ba/EuFe₂As₂ and Co doped Ba₂As₂ 122 compounds using trARPES.

Photoelectron spectroscopy is widely considered to be a surface sensitive method due to the small penetration depth of the free electron like final state into the material for energies of 10–100 eV. For the low photon energy of 6–7 eV used in laser photoemission experiments [11–13] as well as in the present study a bulk sensitivity can be considered [12] due to a larger mean free path of excited electrons. However, on the one hand, a sensitivity to electronic surface states for these small kinetic energies of photoelectrons is well established [14, 15]; on the other hand, combined surface and bulk sensitivity [16] and detection of states at buried interfaces [17] have been reported. Therefore, the degree of surface versus bulk sensitivity might be highly material specific and the photoemission matrix elements need to be considered in detail [18]. The present study investigates 122 compounds with their quasi-two-dimensional electronic structure. Closer inspection

of the dimensionality by ARPES resulted in a considerable k_z dispersion which further increases with doping [19–22]. As will be presented below, the reported phenomena are found to be independent of doping. Therefore, the observed response of the material to optical excitation appears to be rather general for this class of compounds.

2. Experimental details

trARPES experiments were performed on EuFe₂As₂ and BaFe₂As₂ parent compounds and on optimally doped BaFe_{1.85}Co_{0.15}As₂ ($T_c = 23$ K). Single crystals of EuFe₂As₂ were grown by the Bridgman method [23] while the Ba-based compounds were grown from self-flux in an alumina crucible [24]. All samples were cleaved in ultrahigh vacuum ($p < 10^{-10}$ mbar) at $T = 100$ K where the major part of the measurements were carried out. Additional measurements on the parent compounds were performed at 300 K.

A commercial regenerative amplifier, Coherent RegA 9050, generates ultrashort infrared laser pulses of 820 nm wavelength (1.5 eV) with a repetition rate of 300 kHz and pulse duration of 55 fs. The beam is then split in two parts, where one is used to provide the pump pulses and the other one is frequency-doubled and compressed twice to achieve 205 nm wavelength (6 eV) pulses with a duration of 80 fs, used for probing. We detect photoelectrons which are generated by the UV probe pulse using an electron time of flight spectrometer with an acceptance angle of $\pm 3.8^\circ$, which corresponds to a resolution in momentum space of 0.05 \AA^{-1} . An improved momentum resolution can be obtained by employing a recently implemented time of flight spectrometer using a position sensitive detector [25], or by a hemispherical electron analyzer as used, e.g., in [13]. Thereby we monitor the momentum and energy dependent single-particle spectral function in the vicinity of the Fermi level, E_F , as a function of pump–probe delay. Measurements were carried out in normal emission. The laser pulses were incident under 45° with respect to the surface normal. Considering the acceptance angle of the spectrometer we average over 5% of the Brillouin zone around the Γ point. The energy resolution of 50 meV is determined by the time of flight spectrometer and the bandwidth of the probe pulses. The overall temporal resolution was 100 fs [11].

3. Results and discussion

The time-resolved photoelectron intensity of BaFe_{1.85}Co_{0.15}As₂ at the Γ -point is shown in figure 1(a) as function of binding energy and time delay for an incident excitation fluence of $F = 1.4$ mJ cm⁻². After optical excitation, (i) pronounced oscillations modulate the photoemission spectrum around E_F and (ii) optically excited electrons and holes broaden the distribution function around E_F . In this report we disentangle these contributions and discuss the coherent phonon and electron dynamics in sections 3.1 and 3.2, respectively. Figure 1(b) compares spectra taken at $\Delta t = 100$ and 200 fs, corresponding to

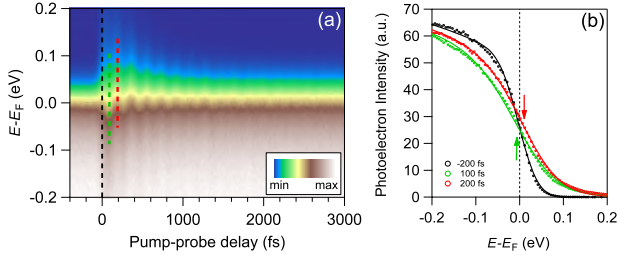


Figure 1. (a) Color coded intensity plot of the trARPES intensity of $\text{BaFe}_{1.85}\text{Co}_{0.15}\text{As}_2$ at the Γ point as a function of binding energy and pump-probe delay, taken with an incident pump fluence of $F = 1.4 \text{ mJ cm}^{-2}$ at $T = 100 \text{ K}$. The red and green dashed lines mark the spectra shown in (b). (b) trARPES spectra for the first minimum (green) and maximum (red) of the oscillation in comparison to a spectrum before excitation (black). The solid lines are fits to the data (see section 3.2). The Fermi level position, E_F , extracted from the fit is indicated by the red and green arrows.

the first minimum and maximum of the oscillations, with a spectrum taken before excitation. Apart from the strong change in the distribution function at E_F after excitation, a shift of the whole Fermi cutoff corresponding to a coherent spectral weight transfer in the vicinity of E_F , which is driven by the coherent oscillations, is observed.

3.1. Coherent phonon dynamics

We start with a discussion of the pronounced oscillations recognized in figure 1(a). The time dependent photoemission intensity integrated for energies $E > E_F$, $I(t)$, is depicted in figure 2(a) for different pumping fluences. This integration yields a rather good signal-to-noise ratio due to the high contrast at the Fermi cutoff. Within the first picosecond after optical excitation, an oscillation with a period close to 200 fs is observed. For $\Delta t > 1.5 \text{ ps}$, an interference pattern is found which indicates the presence of further modes. This is particularly evident for the data at higher fluence. These oscillations are superimposed on a steep rise in integrated intensity after the optical excitation followed by an intensity decrease. In the following we refer to the oscillatory part as the coherent contribution and to the non-oscillatory part as the incoherent contribution to $I(t)$. To determine the coherent contribution, the incoherent contribution was subtracted from $I(t)$. As a first step, the incoherent part was described by a single exponential decay. While this description was adequate at low excitation densities, for higher excitation densities this procedure does not provide a satisfactory background determination. For this reason, we adopted a method consisting of fitting a smooth spline function to the data, which was originally developed for the analysis of extended x-ray absorption fine structure (EXAFS) [26] and was recently used to extract the coherent oscillations of the charge density wave (CDW) amplitude mode in TbTe_3 [27]. This method provides a smooth background while leaving the oscillation unaffected as shown in figure 2(b). For more details see [27]. After background subtraction, fast Fourier transformation (FFT) was used to obtain the frequency spectrum of the coherent contribution, $\Delta I_{\text{coh}}(t)$. Figure 3(a)

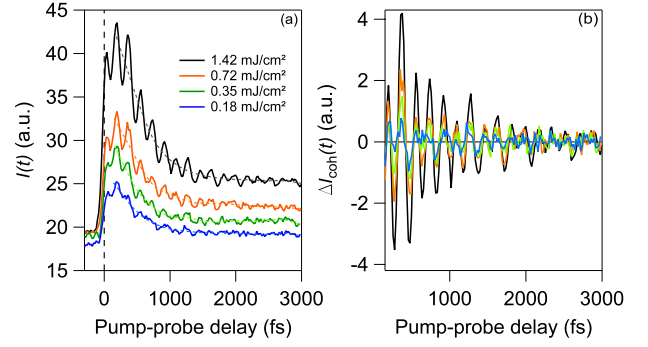


Figure 2. (a) Integrated trARPES intensity of $\text{BaFe}_{1.85}\text{Co}_{0.15}\text{As}_2$ as a function of pump-probe delay for four different fluences measured at 100 K. The dashed lines show the fitted spline function used to obtain background subtraction. (b) The respective background-subtracted oscillations.

depicts the FFTs for the corresponding fluences presenting a sharp intense peak at $\omega_1 = 5.6 \text{ THz}$ ($23 \pm 1 \text{ meV}$) and two weaker modes at $\omega_2 = 3.3 \text{ THz}$ ($14 \pm 1 \text{ meV}$) and $\omega_3 = 2.6 \text{ THz}$ ($11 \pm 1 \text{ meV}$). As discussed below, these features are likely to be fingerprints of coherent lattice vibrations and are observed in trARPES due to the coupling between the electronic system and the coherent phonons. All three modes were found with similar frequencies also in the parent compounds BaFe_2As_2 and EuFe_2As_2 (figure 3(b)), suggesting that these coherent excitations are a general phenomenon in 122 FePns.

The resulting frequencies are summarized in figure 4 as a function of the incident pumping fluence for the three samples under investigation. The open and closed symbols denote data taken at $T = 300 \text{ K}$ and $T = 100 \text{ K}$, respectively. The experimental errors are determined by the point spacing of the FFT which depends on the extent of the respective data set in the time domain. Additional uncertainties arise from the decay of the oscillations in the time domain, which leads to broadening of the peaks in the FFT. We find that the determined FFT frequencies do not vary with the excitation density in all three cases and are temperature independent (see also figure 3(c)). The FFT amplitude for ω_1 in $\text{BaFe}_{1.85}\text{Co}_{0.15}\text{As}_2$ in the lower panel of figure 4 is well described by a linear dependence with fluence. In combination with the fluence independent frequencies, this points to the linear regime of the coherent excitations, showing no indication of anharmonicity within our sensitivity [28].

To determine the geometry and character of the coherent modes, we compare our data with Raman scattering results [29–34] and a theoretical study [7]. By this comparison, we clearly identify the mode ω_1 at 23 meV with the Raman active As A_{1g} phonon mode, corresponding to a displacement of the As atoms perpendicular to the FeAs layers, as sketched in the inset of figure 3(a). This mode has been found in Raman scattering studies of various pnictide 122 compounds [29–34], including BaFe_2As_2 . In addition, coherent excitation of this mode has also been observed in time-resolved reflectivity measurements on Co doped BaFe_2As_2 [9] and in terahertz spectroscopy on BaFe_2As_2 [35]. The frequency was found to be 5.56 THz in

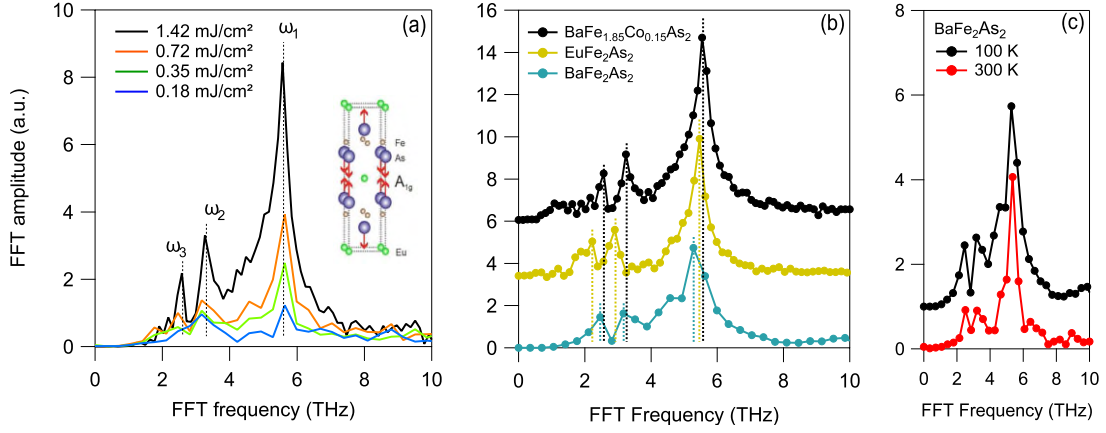


Figure 3. (a) Fast Fourier amplitudes of the data in figure 2 for the corresponding fluences showing the three coherent modes $\omega_1 = 5.6$ THz, $\omega_2 = 3.3$ THz, $\omega_3 = 2.6$ THz. The inset is a sketch of the A_{1g} mode, corresponding to a vertical displacement of the As atoms with respect to the Fe plane. (b) Comparison of the FFTs for BaFe_{1.85}Co_{0.15}As₂, BaFe₂As₂ and EuFe₂As₂ at $T = 100$ K. The traces are vertically offset for clarity. (c) Comparison of the FFTs of BaFe₂As₂ for $T = 300$ and 100 K. All three modes are found to be independent of T .

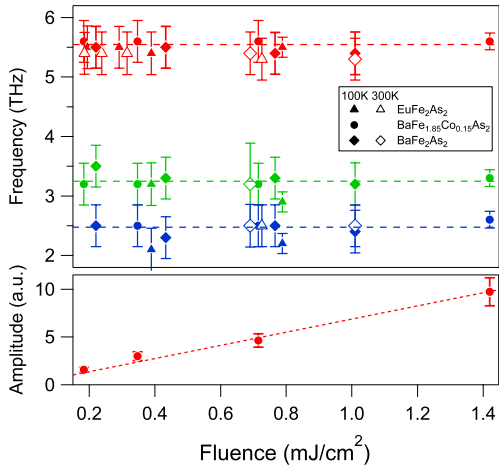


Figure 4. Upper panel: FFT frequencies of the three modes as a function of excitation fluence F for EuFe₂As₂ (triangles), BaFe_{1.85}Co_{0.15}As₂ (circles) and BaFe₂As₂ (diamonds). The open and closed symbols represent data taken at $T = 300$ K and $T = 100$ K, respectively. Error bars are defined by the inter-point spacing of the FFT. The horizontal lines are guides to the eyes. Within error bars, the frequencies of the modes do not depend on the excitation density. Lower panel: FFT amplitude for ω_1 of BaFe_{1.85}Co_{0.15}As₂ as a function of incident pumping fluence. The dashed line is a linear fit to the data.

the first case and 5.5 THz in the latter, which is in agreement with our observation. A more recent study found a coherent excitation of the A_{1g} mode also in SmFeAsO [36], which suggests that the coherent excitation of this mode is a general phenomenon in the FePns. However, the other two modes were not observed with time-resolved optical spectroscopy.

For the excitation of coherent phonons, traditionally two models have been established [37–39], displacive excitation of coherent phonons (DECP) [40] and impulsive stimulated Raman scattering (ISRS) [41]. While the DECP mechanism is supposed to be the main excitation mechanism in opaque media like metals and semi-metals and allows to first order only the excitation of fully symmetric A_1 modes [40], ISRS

is commonly accepted as the excitation process in transparent media like insulators and some semiconductors and allows for the excitation of all Raman active modes [9, 38]. It has been shown that ISRS can also be extended to opaque materials and is the more general description [37]. From the observation of coherently excited phonons here in trARPES, we can conclude on a strong coupling of the coherent vibration to electronic states directly at E_F , as we measure the imprint of the coherent modes on the electronic system.

The assignment of the other two modes is less clear. A possible candidate for the ω_2 mode could be the E_g mode, a shear vibration of the Fe and As atoms within the FeAs plane [33]. On the one hand, this Raman active mode was found at 16 meV [33] corresponding to 3.8 THz, which is considerably higher than the mode ω_2 in our experiment, and this frequency for the E_g mode is consistent with Raman observations of this mode in BaFe₂As₂ [29]. On the other hand, a Raman scattering study on CaFe₂As₂ [42] reported the observation of a mode at 3.35 THz, which could be attributed to the E_g mode. In addition, a recent study of Co doped BaFe₂As₂ using inelastic x-ray scattering found modes close to the BZ center with an energy ≈ 13 meV [43]. These values are all consistent with our observation.

Comparing our frequencies with the calculated phonon dispersion in [7], we see that another possible candidate for the ω_2 mode could be the mode at the X-point around 13 meV, which shows combined in-plane and out-of-plane oscillations with wavevector q equal to the nesting wavevector Q_n and enhanced electron–phonon (e–ph) coupling according to the calculations. The coherent excitation of phonon modes with finite momenta is usually prohibited, as the exciting photons allow only vertical transitions due to their negligible momentum. However, a specific momentum dependent optical excitation probability could in principle generate a transient momentum dependent population of hot charge carriers that could drive also boson modes with finite momenta. Furthermore, contributions of surface phonons or spin excitations [44, 45], which do not show up in the calculations or in Raman spectroscopy, cannot be ruled out.

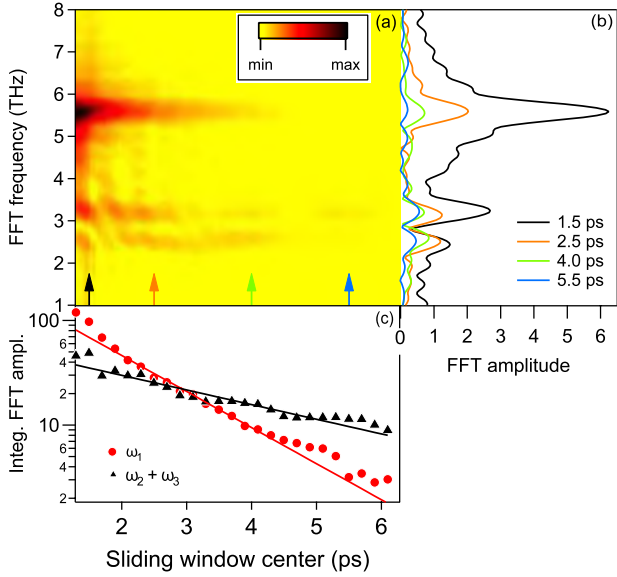


Figure 5. (a) Color coded intensity plot of the swFFT intensity of $\text{BaFe}_{1.85}\text{Co}_{0.15}\text{As}_2$ (at $F = 1.4 \text{ mJ cm}^{-2}$, $T = 100 \text{ K}$) as a function of frequency and time delay of the sliding window center. A sliding window width of 2.4 ps was used. (b) The swFFT corresponding to four different sliding window centers, marked by arrows in (a). (c) Time evolution of the integrated swFFT amplitude of ω_1 and $\omega_2 + \omega_3$ integrated together, plotted on a logarithmic scale. The solid lines are fits to the data.

Regarding the ω_3 mode, the calculation in [7] shows a mode at the zone center around 10 meV which is, however, not Raman active. Furthermore, according to the calculation, this mode couples only weakly to the electronic system and thus would not be observed here. Therefore additional work is required in order to unambiguously clarify the geometry and character of these two modes, ω_2 and ω_3 .

We will now concentrate on the time evolution of the three modes. Considering the FFTs in figure 3, we notice that the mode ω_1 exhibits a considerably broader peak in the frequency domain than the other two modes ω_2 and ω_3 . This indicates a faster relaxation in the time domain of this mode. In order to study this time evolution in more detail, we concentrated on the $\text{BaFe}_{1.85}\text{Co}_{0.15}\text{As}_2$ data using the highest pump fluence of $F = 1.4 \text{ mJ cm}^{-2}$ and applied a sliding window fast Fourier transform (swFFT) analysis, with a time-window of 2.4 ps which allows a frequency resolution of $\sim 0.5 \text{ THz}$, sufficient to resolve the two modes ω_2 and ω_3 that are closest to each other. The intensity of the swFFT signal as function of the transformed frequency and the sliding window center is shown in figure 5(a). No change in the frequency of the modes with time is observed, which is consistent with the harmonic regime of the oscillations concluded above and from figure 4. In addition, the amplitude of ω_1 is indeed damped with a higher decay rate than the amplitudes of the other two modes. This becomes obvious in figure 5(b), where the swFFT intensity corresponding to four different sliding window centers, marked by arrows in figure 5(a), is shown. The integrated swFFT amplitude at the frequencies of the modes is plotted on a logarithmic scale as a function of the window position in figure 5(c). Note that due to

interference effects between ω_2 and ω_3 , combined amplitudes corresponding to these two modes were integrated. The integrated swFFT amplitude of both ω_1 and $\omega_2 + \omega_3$ shows a clear linear behavior in the logarithmic plot. By fitting single exponential decay functions to the respective amplitude time evolutions (solid lines), we determine $\tau_1 = 1.2 \pm 0.1 \text{ ps}$ and $\tau_{\omega_2+\omega_3} = 3.1 \pm 0.4 \text{ ps}$ as decay times. We will now discuss the different relaxation times for the mode ω_1 and the modes ω_2 and ω_3 . The relaxation of coherently excited phonons occurs through both pure dephasing and population decay of the excited modes. While the pure dephasing takes place mainly by scattering at crystal defects and e-ph interaction, the population decay is governed by anharmonic phonon-phonon (ph-ph) interaction [46]. The scattering with crystal defects is unlikely to explain the different decay behavior of different modes within the same crystal, assuming a homogeneous excitation density of these modes. This could be different for, e.g., surface modes. The other two relaxation processes can be distinguished by their temperature and fluence dependences. On the one hand, relaxation by anharmonic ph-ph decay into two acoustic phonons shows an increase in decay rate with increasing temperature [38, 46]. This is not observed in our case, as we have not found an increase of the widths of the peaks in the FFT spectra for the higher temperature as shown in figure 3(c). On the other hand, scattering of coherent phonons with excited carriers by e-ph coupling is highly dependent on the density of excited carriers and thus on the excitation density, which leads to a faster decay at higher excitation densities [28, 46]. This is indeed observed in the data in figure 3(a), where we find an increase with fluence of the linewidth of ω_1 . Therefore, we conclude that the dominant relaxation channel for the coherent oscillations is the coupling to excited carriers by e-ph scattering. The shorter lifetime of the mode ω_1 compared to the other two modes thus indicates a stronger coupling to the electronic system for the mode ω_1 . This is consistent with the lower amplitude of the other two modes, as e-ph coupling is the key parameter for both the generation and the detection of coherent phonons in trARPES and, as a consequence, the amplitude of coherent phonons in the detected signal scales with the coupling strength.

Interestingly, the relaxation that we have found for the mode ω_1 is clearly faster than in time-resolved optical reflectivity measurements, where the A_{1g} mode was found to relax with a time constant of $\tau_{A_{1g}} \sim 2.5 \text{ ps}$ [9]. This might be explained by a difference in crystal quality, exhibiting fewer crystal defects in the optical pump-probe experiments. Another possibility might be the different detection technique used. Whereas optical reflectivity probes the entire region of the optical penetration depth of several tens of nanometers, photoelectron spectroscopy is a surface sensitive technique. Thus, the coherent phonons in the subsurface region might exhibit a faster relaxation than in the bulk of the lattice.

3.2. Dynamics of the electronic system

So far we have analyzed the oscillations in time dependent photoelectron intensity. As has been mentioned above, two further phenomena are observed in the data presented in

figure 1. These are (i) the photo-excited distribution of electrons and holes and (ii) a variation of the high energy cutoff of the spectra. While the distributions of hot charge carriers have already been discussed before in detail for other materials [47–51] the clear change in the high energy cutoff is less established. Here we report the results of an analysis based on the assumption that these two phenomena can be described by the combination of a thermalized hot electron distribution function and a transient modification of the chemical potential. The fits presented in figure 1(b) are the result of this model approach and describe the data very well. These fits have been performed as a function of time delay and the resulting hot electron temperature $T_e(t)$ and chemical potential $\mu(t)$ are depicted in figures 6(a) and (b) respectively. Note that for this analysis a constant auxiliary density of states was assumed and non-thermal hot electrons which occur before the thermalization of the electronic system close to t_0 were neglected here for simplicity⁹. We find a strong modulation of $\mu(t)$ which indicates that the intensity oscillations discussed above originate from a time dependent change, $\mu = \mu(t)$, and that the coherent phonon excitation modifies the chemical potential. Although details of this phenomenon remain to be analyzed in future work we tentatively explain the changes in $\mu(t)$ as a consequence of the modulation of the electronic structure in response to coherent phonons [14, 16, 17, 52, 53]. Due to the significant variation of the electronic density of states near E_F in the multiband structure of FePns systems [54], charge neutrality might well require a transient readjustment of μ to the instantaneous position of the electron and hole pockets at X and Γ , respectively.

To describe the time dependent change of T_e we employ a three temperature model (3TM) as used before for the high T_c superconductor $\text{Bi}_2\text{Sr}_2\text{CaCu}_2\text{O}_{8+\delta}$ (BSCCO) [48]. This description gives a reasonable agreement with the obtained $T_e(t)$ as shown in figure 6(a). A similar analysis within the same 3TM has been recently performed for FePns using time-resolved optical reflectivity measurements [55]. The 3TM describes the preferential coupling of the optically excited hot electron distribution with temperature T_e to a more strongly coupled subset of phonon modes with temperature T_p , which subsequently couple on a longer timescale to the rest of the lattice modes with temperature T_l . The following set of coupled differential equations is used [48, 56]:

$$\frac{\partial T_e}{\partial t} = -H(T_e, T_p) + \frac{S}{C_e} \quad (1)$$

$$\frac{\partial T_p}{\partial t} = +\frac{C_e}{C_p} H(T_e, T_p) - \frac{T_p - T_l}{\tau_\beta} \quad (2)$$

$$\frac{\partial T_l}{\partial t} = +\frac{C_p}{C_l} \frac{T_p - T_l}{\tau_\beta}. \quad (3)$$

The source term S is a Gaussian excitation pulse with an FWHM of 55 fs and an energy density determined by the absorbed fluence distributed over the optical penetration

⁹ For several systems we have observed and partly included such a subsystem of non-thermalized electrons [47, 48].

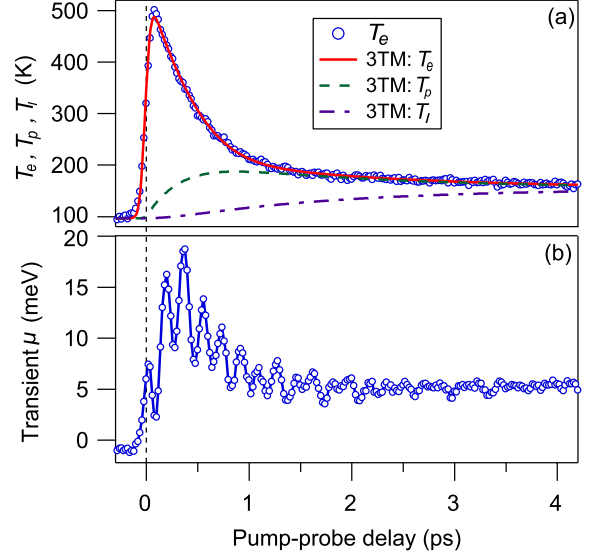


Figure 6. Time dependent electronic temperature T_e (a) and chemical potential μ (b) determined by fitting the transient trARPES spectra shown in figure 1 (see text). The results of a fit with a three temperature model (3TM) for T_e (red), the temperature of a heat bath of more strongly coupled phonon modes T_p (dashed green) and the lattice temperature T_l (dashed-dotted dark violet) are also shown in (a).

depth. The specific heat of the electrons is determined by $C_e = \gamma_e T_e$, with the electronic specific heat coefficient γ_e . For the specific heats of the hot phonons and the rest of the phonons, the Einstein model with an ω_0 mode is used, $C_p = 3f\hbar\omega_0 \frac{\partial n}{\partial T}|_{T_p}$ and $C_l = 3(1-f)\hbar\omega_0 \frac{\partial n}{\partial T}|_{T_l}$, where $n = (e^{\hbar\omega_0/k_B T} - 1)^{-1}$ is the Bose–Einstein distribution function. The parameter f is the fraction of modes that are more strongly coupled to the electrons. The anharmonic decay (responsible for the loss of oscillation signal) of the respective subset of hot phonons to the remaining, more weakly coupled, phonons is described by τ_β . For the energy transfer from the electrons to the more strongly coupled phonons, the formula derived by Allen [56] is used,

$$H(T_e, T_p) = \frac{3\hbar\lambda\langle\omega^2\rangle}{\pi k_B} \frac{T_e - T_p}{T_e}, \quad (4)$$

where $\lambda\langle\omega^2\rangle$ is the second moment of the Eliashberg e–ph coupling function $\alpha^2 F(\omega)$. The e–ph coupling to the weakly coupled fraction $(1-f)$ barely influences the evolution of T_e and has therefore been neglected. Electronic diffusion processes can be assumed not to be essential here as the electric and thermal conductivities are strongly reduced along the longer c -axis due to the layered, quasi-2D structure of the FePns [57, 58].

Naturally, the description of the phonon system with a simple Einstein mode is a strong simplification and a proper choice of the mode energy influences the result of the simulation. To provide an estimate for the frequency ω_0 , we consider the phonon spectrum of the 122 FeAs compounds. The calculated phonon spectrum extends up to ~ 35 meV as derived in several calculations [8, 43, 54] and supported by

Table 1. Fitting parameters of the 3TM. The left and right values for f and $\lambda\langle\omega^2\rangle$ correspond to choices of $\omega_0 = 10$ meV and 30 meV, respectively.

Compound	f	$\lambda\langle\omega^2\rangle$ (meV ²)	τ_β (ps)
EuFe ₂ As ₂	0.43–0.38	56–65	2.9 ± 0.3
BaFe _{1.85} Co _{0.15} As ₂	0.48–0.43	46–55	3.3 ± 0.5
BaFe ₂ As ₂	~0.45	30–46	~3.5

experiments [54, 59, 60] with the strongest contributions to $\alpha^2F(\omega)$ between 10 and 30 meV [8].

The 3TM was fitted to the transient T_e for various values of ω_0 between 10 and 30 meV. The resulting values for the parameters of the model are summarized in table 1 for the three investigated compounds. For f and $\lambda\langle\omega^2\rangle$, the left and right values are for choices of $\omega_0 = 10$ meV and 30 meV, respectively. An exemplary fit of the electronic temperature T_e using $\omega_0 = 18$ meV is shown in figure 6(a) for the Co doped sample as solid line, which shows excellent agreement with the measured data. For other choices of ω_0 , similar good agreement to the data is found. The temperatures of hot phonons (T_p) and other phonons (T_l) derived from the model are shown as dashed and dash-dotted lines, respectively.

The values determined for $\lambda\langle\omega^2\rangle$ can be compared to recently published values for the e–ph coupling strength obtained from optical pump–probe experiments. Mansart *et al* [55] report a value of $\lambda\langle\omega^2\rangle \approx 64$ meV² for almost optimally doped BaFe_{2–x}Co_xAs₂, which was determined by the 3TM. Stojchevska *et al* [10] derived a somewhat higher value of $\lambda\langle\omega^2\rangle = 110 \pm 10$ meV² for SrFe₂As₂ from the temperature dependence of quasiparticle relaxation times and for SmFeAsO_{1–x}F_x an even larger value of $\lambda\langle\omega^2\rangle = 135 \pm 10$ meV² was reported [36]. In general, our results are compatible with the weak e–ph coupling found in the FePns and indicate even weaker coupling for BaFe₂As₂ compounds than in EuFe₂As₂. However, one has to bear in mind that the performed analysis assumes a thermalized electronic system and systematically neglects non-thermal electrons. As thermalization of non-thermal hot electrons leads to an additional heating of the thermalized electron distribution, this process can counteract the energy transfer to the lattice and leads to a slower energy relaxation of the thermalized electrons. Thus, analysis of only the thermalized part of the electronic distribution might considerably underestimate the e–ph coupling especially at early times.

The fraction $f \approx 0.4$ of preferentially coupled modes is in agreement with the observations of Mansart *et al* [55], and is considerably higher than that found in BSCCO of $f \approx 0.2$ [48]. Here we follow the explanation given by Mansart *et al*, who suggest that this stronger selectivity of e–ph coupling in the cuprates can be explained by the stronger 2D character of the cuprates, which could favor selective coupling to specific modes. The FePns and especially Co doped 122 compounds are characterized by a stronger interlayer coupling and a more 3D character [19], which might lead to a less selective e–ph coupling [55]. The equilibration time τ_β of the hot phonon distribution with the rest of the lattice modes is considerably faster here than in the optical reflectivity measurements by Mansart *et al*, who

report $\tau_\beta \sim 5$ –7 ps. This faster relaxation of excited phonon modes observed in trARPES measurements compared to optical reflectivity is consistent with the faster relaxation of the coherently excited phonon modes discussed earlier and indicates different phonon relaxation behaviors in the bulk and the surface/subsurface regions, respectively. In addition, the excitation densities in the experiments by Mansart *et al* were a factor of two to three larger than here, and an increase of τ_β with fluence was observed [55].

Based on our results for $\lambda\langle\omega^2\rangle$ we can estimate the value of the e–ph coupling constant λ for a particular value of ω . Considering the coherently excited A_{1g} mode at 23 meV, which showed enhanced coupling in calculations, we find $\lambda < 0.15$ for all compounds. This estimate is in agreement with calculations [7, 8] of various FePns compounds, which report average values of $\lambda < 0.35$. Taking the mean of the phonon DOS as reference, λ gets even smaller in agreement with other publications. Even if we consider the lowest coupled modes around 12 meV to be most important for e–ph coupling, λ does not exceed a value of 0.5. Similar small values for λ have been found in the cuprates [48], which might suggest limited importance of e–ph coupling for the pairing mechanism in both classes of material.

4. Conclusion

Femtosecond time- and angle-resolved photoelectron spectroscopy was demonstrated to be a powerful tool to investigate the response of the electronic system in the vicinity of the Fermi level. In this study we could separate transient changes in the electron distribution function and the chemical potential for various 122 FePns compounds. The first was analyzed by a simplified three temperature model. In agreement with earlier time-resolved optical studies we conclude on a rather small momentum-averaged electron–phonon coupling constant $\lambda < 0.15$, which could suggest a limited importance of e–ph coupling for the Cooper pair formation in these systems. The transient chemical potential is explained to be the consequence of charge neutrality in the probed region of the material while the electronic system is in a non-equilibrium state characterized by hot electrons and coherent as well as incoherent phonons. Such changes in the chemical potential can be expected to be a general phenomenon; however, we consider that the two band nature of the 122 FePns compounds enhances the effect in comparison to a single band system. The pronounced effect of coherent phonons on the electronic structure near E_F demonstrates vivid electron–phonon coupling but the assignment of the two observed lower frequency excitations beside the A_{1g} mode

requires further attention. Future studies as a function of doping might provide more insight into the origin of the changes in the chemical potential as well as the material specificity of all observed coherent phonon modes.

Acknowledgments

Funding from the Deutsche Forschungsgemeinschaft within SPP 1458 is gratefully acknowledged. RC Acknowledges the Alexander von Humboldt Foundation. We thank Hermann Dürr and Lilia Boeri for fruitful discussions.

References

- [1] Kamihara Y, Watanabe T, Hirano M and Hosono H 2008 Iron-based layered superconductor $\text{LaO}_{1-x}\text{F}_x\text{FeAs}$ ($x = 0.05\text{--}0.12$) with $T_c = 26$ K *J. Am. Chem. Soc.* **130** 3296
- [2] Stewart G R 2011 Superconductivity in iron compounds *Rev. Mod. Phys.* **83** 1589–652
- [3] Kroll T *et al* 2008 Electronic structure of $\text{LaFeAsO}_{1-x}\text{F}_x$ from x-ray absorption spectroscopy *Phys. Rev. B* **78** 220502
- [4] Bondino F *et al* 2008 Evidence for strong itinerant spin fluctuations in the normal state of $\text{CeFeAsO}_{0.89}\text{F}_{0.11}$ iron-oxypnictide superconductors *Phys. Rev. Lett.* **101** 267001
- [5] Bondino F *et al* 2010 Electronic structure of $\text{CeFeAsO}_{1-x}\text{F}_x$ ($x = 0, 0.11, \text{ and } 0.12$) *Phys. Rev. B* **82** 014529
- [6] Malaeb W *et al* 2008 Electronic structure and electron correlation in $\text{LaFeAsO}_{1-x}\text{F}_x$ and $\text{LaFePO}_{1-x}\text{F}_x$ *J. Phys. Soc. Japan* **77** 093714
- [7] Boeri L, Dolgov O V and Golubov A A 2008 Is $\text{LaFeAsO}_{1-x}\text{F}_x$ an electron–phonon superconductor? *Phys. Rev. Lett.* **101** 026403
- [8] Boeri L, Calandra M, Mazin I I, Dolgov O V and Mauri F 2010 Effects of magnetism and doping on the electron–phonon coupling in BaFe_2As_2 *Phys. Rev. B* **82** 020506
- [9] Mansart B, Boschetto D, Savoia A, Rullier-Albenque F, Forget A, Colson D, Rousse A and Marsi M 2009 Observation of a coherent optical phonon in the iron pnictide superconductor $\text{Ba}(\text{Fe}_{1-x}\text{Co}_x)_2\text{As}_2$ ($x = 0.06$ and 0.08) *Phys. Rev. B* **80** 172504
- [10] Stojchevska L, Kusar P, Mertelj T, Kabanov V V, Lin X, Cao G H, Xu Z A and Mihailovic D 2010 Electron–phonon coupling and the charge gap of spin-density wave iron-pnictide materials from quasiparticle relaxation dynamics *Phys. Rev. B* **82** 012505
- [11] Rettig L, Cortés R, Thirupathaiah S, Gegenwart P, Jeevan H S, Wolf M, Fink J and Bovensiepen U 2012 Ultrafast momentum-dependent response of electrons in antiferromagnetic EuFe_2As_2 driven by optical excitation *Phys. Rev. Lett.* **108** 097002
- [12] Kiss T *et al* 2005 Photoemission spectroscopic evidence of gap anisotropy in an f-electron superconductor *Phys. Rev. Lett.* **94** 057001
- [13] Koralek J D *et al* 2006 Laser based angle-resolved photoemission, the sudden approximation, and quasiparticle-like spectral peaks in $\text{Bi}_2\text{Sr}_2\text{CaCu}_2\text{O}_{8+\delta}$ *Phys. Rev. Lett.* **96** 017005
- [14] Loukakos P A, Lisowski M, Bihlmayer G, Blügel S, Wolf M and Bovensiepen U 2007 Dynamics of the self-energy of the Gd(0001) surface state probed by femtosecond photoemission spectroscopy *Phys. Rev. Lett.* **98** 097401
- [15] Bovensiepen U, Petek H and Wolf M 2011 *Current Developments (Dynamics in Solid State Surfaces and Interfaces vol 1)* (Weinheim: Wiley)
- [16] Perfetti L, Loukakos P A, Lisowski M, Bovensiepen U, Berger H, Biermann S, Cornaglia P S, Georges A and Wolf M 2006 Time evolution of the electronic structure of 1T--TaS_2 through the insulator–metal transition *Phys. Rev. Lett.* **97** 067402
- [17] Rettig L, Kirchmann P S and Bovensiepen U 2012 Ultrafast dynamics of occupied quantum well states in $\text{Pb/Si}(111)$ *New J. Phys.* **14** 023047
- [18] Schattke W 2000 Electron scattering states for low-energy spectroscopies *Prog. Surf. Sci.* **64** 89
- [19] Vilmercati P *et al* 2009 Evidence for three-dimensional fermi-surface topology of the layered electron-doped iron superconductor $\text{Ba}(\text{Fe}_{1-x}\text{Co}_x)_2\text{As}_2$ *Phys. Rev. B* **79** 220503
- [20] Fink J *et al* 2009 Electronic structure studies of BaFe_2As_2 by angle-resolved photoemission spectroscopy *Phys. Rev. B* **79** 155118
- [21] Thirupathaiah S *et al* 2010 Orbital character variation of the fermi surface and doping dependent changes of the dimensionality in $\text{BaFe}_{2-x}\text{Co}_x\text{As}_2$ from angle-resolved photoemission spectroscopy *Phys. Rev. B* **81** 104512
- [22] Thirupathaiah S *et al* 2011 Dissimilarities between the electronic structure of chemically doped and chemically pressurized iron pnictides from an angle-resolved photoemission spectroscopy study *Phys. Rev. B* **84** 014531
- [23] Jeevan H S, Hossain Z, Kasinathan D, Rosner H, Geibel C and Gegenwart P 2008 Electrical resistivity and specific heat of single-crystalline EuFe_2As_2 : a magnetic homologue of SrFe_2As_2 *Phys. Rev. B* **78** 052502
- [24] Hardy F, Adelman P, Wolf T, Löhneysen H v and Meingast C 2009 Large anisotropic uniaxial pressure dependencies of T_c in single crystalline $\text{Ba}(\text{Fe}_{0.92}\text{Co}_{0.08})_2\text{As}_2$ *Phys. Rev. Lett.* **102** 187004
- [25] Kirchmann P S, Rettig L, Nandi D, Lipowski U, Wolf M and Bovensiepen U 2008 A time-of-flight spectrometer for angle-resolved detection of low energy electrons in two dimensions *Appl. Phys. A* **91** 211–7
- [26] Lee P A, Citrin P H, Eisenberger P and Kincaid B M 1981 Extended x-ray absorption fine structure its strengths and limitations as a structural tool *Rev. Mod. Phys.* **53** 769–806
- [27] Schmitt F, Kirchmann P S, Bovensiepen U, Moore R G, Chu J-H, Lu D H, Rettig L, Wolf M, Fisher I R and Shen Z-X 2011 Ultrafast electron dynamics in the charge density wave material TbTe_3 *New J. Phys.* **13** 26
- [28] Hase M, Kitajima M, Nakashima S and Mizoguchi K 2002 Dynamics of coherent anharmonic phonons in bismuth using high density photoexcitation *Phys. Rev. Lett.* **88** 067401
- [29] Chauvière L, Gallais Y, Cazayous M, Sacuto A, Méasson M A, Colson D and Forget A 2009 Doping dependence of the lattice dynamics in $\text{Ba}(\text{Fe}_{1-x}\text{Co}_x)_2\text{As}_2$ studied by Raman spectroscopy *Phys. Rev. B* **80** 094504
- [30] Chauvière L, Gallais Y, Cazayous M, Méasson M A, Sacuto A, Colson D and Forget A 2011 Raman scattering study of spin-density-wave order and electron–phonon coupling in $\text{Ba}(\text{Fe}_{1-x}\text{Co}_x)_2\text{As}_2$ *Phys. Rev. B* **84** 104508
- [31] Choi K-Y, Wulferding D, Lemmens P, Ni N, Bud’ko S L and Canfield P C 2008 Lattice and electronic anomalies of CaFe_2As_2 studied by Raman spectroscopy *Phys. Rev. B* **78** 212503
- [32] Kumar P *et al* 2011 Raman evidence for the superconducting gap and spin–phonon coupling in the superconductor $\text{Ca}(\text{Fe}_{0.95}\text{Co}_{0.05})_2\text{As}_2$ *J. Phys.: Condens. Matter* **23** 255403
- [33] Litvinchuk A P, Hadjiev V G, Iliev M N, Bing Lv, Guloy A M and Chu C W 2008 Raman-scattering study of $\text{K}_x\text{Sr}_{1-x}\text{Fe}_2\text{As}_2$ ($x = 0.0, 0.4$) *Phys. Rev. B* **78** 060503

- [34] Sugai S, Mizuno Y, Kiho K, Nakajima M, Lee C H, Iyo A, Eisaki H and Uchida S 2011 Erratum: Pairing symmetry of the multiorbital pnictide superconductor $\text{BaFe}_{1.84}\text{Co}_{0.16}\text{As}_2$ from Raman scattering *Phys. Rev. B* **83** 019903
- [35] Kim K W, Pashkin A, Schäfer H, Beyer M, Porer M, Wolf T, Bernhard C, Demsar J, Huber R and Leitenstorfer A 2012 Ultrafast transient generation of spin-density-wave order in the normal state of BaFe_2As_2 driven by coherent lattice vibrations *Nature Mater.* **11** 497–501
- [36] Mertelj T, Kusar P, Kabanov V V, Stojchevska L, Zhigadlo N D, Katrych S, Bukowski Z, Karpinski J, Weyeneth S and Mihailovic D 2010 Quasiparticle relaxation dynamics in spin-density-wave and superconducting $\text{SmFeAsO}_{1-x}\text{F}_x$ single crystals *Phys. Rev. B* **81** 224504
- [37] Garrett G A, Albrecht T F, Whitaker J F and Merlin R 1996 Coherent THz phonons driven by light pulses and the Sb problem: What is the mechanism? *Phys. Rev. Lett.* **77** 3661
- [38] Hase M, Ishioka K, Demsar J, Ushida K and Kitajima M 2005 Ultrafast dynamics of coherent optical phonons and nonequilibrium electrons in transition metals *Phys. Rev. B* **71** 184301
- [39] Ishioka K and Misochko O V 2010 Coherent lattice oscillations in solids and their optical control *Progress in Ultrafast Intense Laser Science (Springer Series in Chemical Physics vol 98)* (Berlin: Springer)
- [40] Zeiger H J, Vidal J, Cheng T K, Ippen E P, Dresselhaus G and Dresselhaus M S 1992 Theory for displacive excitation of coherent phonons *Phys. Rev. B* **45** 768–78
- [41] Yan Y X, Gamble E B and Nelson K A 1985 Impulsive stimulated scattering: general importance in femtosecond laser pulse interactions with matter, and spectroscopic applications *J. Chem. Phys.* **83** 5391
- [42] Litvinchuk A P, Bing Lv and Chu C W 2011 Raman scattering study of electron-doped $\text{Pr}_x\text{Ca}_{1-x}\text{Fe}_2\text{As}_2$ superconductors *Phys. Rev. B* **84** 092504
- [43] Reznik D *et al* 2009 Phonons in doped and undoped BaFe_2As_2 investigated by inelastic x-ray scattering *Phys. Rev. B* **80** 214534
- [44] Melnikov A, Povolotskiy A and Bovensiepen U 2008 Magnon-enhanced phonon damping at $\text{Gd}(0001)$ and $\text{Tb}(0001)$ surfaces using femtosecond time-resolved optical second-harmonic generation *Phys. Rev. Lett.* **100** 247401
- [45] Inosov D S *et al* 2010 Normal-state spin dynamics and temperature-dependent spin-resonance energy in optimally doped $\text{BaFe}_{1.85}\text{Co}_{0.15}\text{As}_2$ *Nature Phys.* **6** 178–81
- [46] Hase M and Kitajima M 2012 Interaction of coherent phonons with defects and elementary excitations *J. Phys.: Condens. Matter* **22** 073201
- [47] Lisowski M, Loukakos P A, Bovensiepen U, Stähler J, Gahl C and Wolf M 2004 Ultra-fast dynamics of electron thermalization, cooling and transport effects in $\text{Ru}(001)$ *Appl. Phys. A* **78** 165–76
- [48] Perfetti L, Loukakos P A, Lisowski M, Bovensiepen U, Eisaki H and Wolf M 2007 Ultrafast electron relaxation in superconducting $\text{Bi}_2\text{Sr}_2\text{CaCu}_2\text{O}_{8+\delta}$ by time-resolved photoelectron spectroscopy *Phys. Rev. Lett.* **99** 197001
- [49] Fann W S, Storz R, Tom H W K and Bokor J 1992 Electron thermalization in gold *Phys. Rev. B* **46** 13592
- [50] Del Fatti N, Voisin C, Achermann M, Tzortzakakis S, Christofilos D and Vallée F 2000 Nonequilibrium electron dynamics in noble metals *Phys. Rev. B* **61** 16956–66
- [51] Rhié H-S, Dürr H A and Eberhardt W 2003 Femtosecond electron and spin dynamics in $\text{Ni}/\text{W}(110)$ films *Phys. Rev. Lett.* **90** 247201
- [52] Schmitt F *et al* 2008 Effect of the amplitude mode and the transient melting of a charge density wave on the electronic structure of TbTe_3 *Science* **321** 1649
- [53] Schmitt F, Kirchmann P S, Bovensiepen U, Moore R G, Chu J-H, Lu D H, Rettig L, Wolf M, Fisher I R and Shen Z-X 2011 Ultrafast electron dynamics in the charge density wave material TbTe_3 *New J. Phys.* **13** 063022
- [54] Zbiri M, Schober H, Johnson M R, Rols S, Mittal R, Su Y, Rotter M and Johrendt D 2009 *Ab initio* lattice dynamics simulations and inelastic neutron scattering spectra for studying phonons in BaFe_2As_2 : effect of structural phase transition, structural relaxation, and magnetic ordering *Phys. Rev. B* **79** 064511
- [55] Mansart B, Boschetto D, Savoia A, Rullier-Albenque F, Bouquet F, Papalazarou E, Forget A, Colson D, Rousse A and Marsi M 2010 Ultrafast transient response and electron-phonon coupling in the iron-pnictide superconductor $\text{Ba}(\text{Fe}_{1-x}\text{Co}_x)_2\text{As}_2$ *Phys. Rev. B* **82** 024513
- [56] Allen P B 1987 Theory of thermal relaxation of electrons in metals *Phys. Rev. Lett.* **59** 1460–3
- [57] Tanatar M A, Ni N, Martin C, Gordon R T, Kim H, Kogan V G, Samolyuk G D, Bud'ko S L, Canfield P C and Prozorov R 2009 Anisotropy of the iron pnictide superconductor $\text{Ba}(\text{Fe}_{1-x}\text{Co}_x)_2\text{As}_2$ ($x = 0.074$, $T_c = 23$ K) *Phys. Rev. B* **79** 094507
- [58] Reid J-Ph, Tanatar M A, Luo X G, Shakeripour H, Doiron-Leyraud N, Ni N, Bud'ko S L, Canfield P C, Prozorov R and Taillefer L 2010 Nodes in the gap structure of the iron arsenide superconductor $\text{Ba}(\text{Fe}_{1-x}\text{Co}_x)_2\text{As}_2$ from *c*-axis heat transport measurements *Phys. Rev. B* **82** 064501
- [59] Hahn S E *et al* 2009 Influence of magnetism on phonons in CaFe_2As_2 as seen via inelastic x-ray scattering *Phys. Rev. B* **79** 220511
- [60] Mittal R *et al* 2009 Measurement of anomalous phonon dispersion of CaFe_2As_2 single crystals using inelastic neutron scattering *Phys. Rev. Lett.* **102** 217001